γ-ray spectroscopy of neutron-deficient ^{123}Ce

J. F. Smith,[1,2,*] L. J. Angus,[1,2] E. S. Paul,[3] C. J. Chiara,[4,†] M. P. Carpenter,[5] H. J. Chantler,[3,‡] P. T. W. Choy,[3] C. N. Davids,[5] M. Devlin,[6] D. B. Fossan,[7,§] S. J. Freeman,[8] R. V. F. Janssens,[5] N. S. Kelsall,[9] T. Koike,[7,‖] D. R. LaFosse,[7] D. G. Sarantites,[4] D. Seweryniak,[5] K. Starosta,[10] R. Wadsworth,[9] and A. N. Wilson[11]

[1]*School of Engineering, University of the West of Scotland, Paisley PA1 2BE, United Kingdom*
[2]*Scottish Universities Physics Alliance*
[3]*Oliver Lodge Laboratory, University of Liverpool, Liverpool L69 7ZE, United Kingdom*
[4]*Department of Chemistry, Washington University, St. Louis, Missouri 63130, USA*
[5]*Physics Division, Argonne National Laboratory, Argonne, Illinois 60439, USA*
[6]*LANSCE-NS, Los Alamos National Laboratory, Los Alamos, New Mexico 87545, USA*
[7]*Department of Physics and Astronomy, State University of New York at Stony Brook, Stony Brook, New York 11794, USA*
[8]*School of Physics and Astronomy, University of Manchester, Manchester M13 9PL, United Kingdom*
[9]*Department of Physics, University of York, Heslington, York YO10 5DD, United Kingdom*
[10]*Department of Chemistry, Simon Fraser University, Burnaby, British Columbia V5A 156, Canada*
[11]*Research School of Physics and Engineering, Australian National University, Canberra ACT 0200, Australia*

(Received 23 May 2012; revised manuscript received 7 July 2012; published 4 September 2012)

Excited states have been identified in the very neutron-deficient $Z = 58$ nucleus ^{123}Ce. This is the most neutron-deficient odd-A cerium isotope in which excited states have been identified. The states have been unambiguously assigned to ^{123}Ce by detecting de-excitation γ rays in coincidence with evaporated charged particles and neutrons. Three rotational bands, each consisting of at least eight $E2$ transitions, have been observed. The bands have tentatively been assigned to be based on neutrons in $g_{7/2}$ and $h_{11/2}$ orbitals. Two of the bands have been assigned to be signature partners, although no interband transitions have been observed. The aligned angular momenta of the bands have been studied in comparison with neighboring nuclei and with the results of Woods-Saxon cranking calculations. Observation of the deformation-dependent $\pi(h_{11/2})^2$ quasiparticle alignment at 0.36 MeV/$\hbar$ in each of the bands suggests a quadrupole deformation of $\beta_2 \simeq 0.3$, in good agreement with theoretical predictions for the suggested possible configuration assignments.

DOI: 10.1103/PhysRevC.86.034303 PACS number(s): 21.10.Re, 23.20.Lv, 27.60.+j, 29.30.Kv

I. INTRODUCTION

It is important to study nuclei far from stability in order to look for unusual or unexpected changes in structure caused by the large excess of neutrons or protons [1,2]. One of the best techniques to study the structure of such nuclei is γ-ray spectroscopy, from which the identification of just the lowest few excited states can reveal a wealth of information. This is especially true for deformed nuclei where the states form rotational bands. Moments of inertia and level spacings can be used to infer deformation, and low-lying quasiparticle alignments can help identify the orbitals involved in the configuration underlying the rotational states.

The lightest known $Z = 58$ cerium isotopes, with $A \lesssim 124$, are good subjects of study in this respect. The cerium isotopes that have been studied to date, with $A \lesssim 128$, are known to be well deformed [3–5], with quadrupole deformation parameters $\beta_2 \simeq 0.25 - 0.30$. The level schemes of these nuclei are dominated by rotational bands built on the ground states and on low-lying excited states. In the cerium isotopes with $121 \leqslant A \leqslant 133$ ($63 \leqslant N \leqslant 75$), the proton Fermi levels lie in the prolate-driving, low-Ω, $h_{11/2}$ orbitals, and the neutron Fermi levels are located in the higher-Ω orbitals of the $h_{11/2}$ subshell. As N decreases from ~75, the valence neutrons occupy orbitals that are progressively more prolate-driving, increasing the quadrupole deformation. This trend is supported by theoretical calculations [6,7] which predict that the deformation will reach a maximum in the odd-A isotopes for $N = 63$, ^{121}Ce. From experimental measurements, the deformations of the odd-A cerium isotopes appear to increase, down to the lightest isotope studied, ^{125}Ce [4]. The cranked shell model predicts that rotational alignments of pairs of both neutrons and protons from the $h_{11/2}$ subshell will occur at relatively low rotational frequencies in these nuclei. The precise details, such as the alignment frequencies, are dependent on the underlying quasiparticle configurations and on the deformation. An experimental study of the alignments can therefore provide information about both the orbitals near the Fermi surface and the overall nuclear shape.

In the present work, an experiment has been carried out using Gammasphere [8], together with the Washington University Microball [9,10] and Neutron Shell [11,12] and the Argonne Fragment Mass Analyzer [13], in order to study excited states in the very neutron-deficient cerium isotopes. The observation of excited states in ^{122}Ce in this experiment

*john.f.smith@uws.ac.uk
†Present address: Department of Chemistry and Biochemistry, University of Maryland, College Park, Maryland 20742, USA.
‡Present address: Addenbrookes Hospital, Department of Medical Physics, Cambridge CB2 2QQ, United Kingdom.
§Deceased.
‖Present address: Graduate School of Science, Tohoku University, Sendai 980-8578, Japan.

has been reported elsewhere [14]. The present paper describes the identification of excited states in ^{123}Ce. Three sequences of at least eight $E2$ transitions have been assigned to ^{123}Ce, which tentatively extend to spins of around $43/2\,\hbar$. Previous experimental studies of the neutron-deficient cerium isotopes are summarized in Sec. II, experimental details and data-analysis methods used in the present work are given in Secs. III and IV, and the results are presented and discussed in Secs. V and VI.

II. PREVIOUS SPECTROSCOPY OF CERIUM ISOTOPES

The neutron-deficient cerium isotopes with $124 \leqslant A \leqslant 132$ have all been well studied in γ-ray spectroscopy experiments. Details are given in the following references: ^{124}Ce [4]; ^{125}Ce [4,15,16]; ^{126}Ce [5,17]; ^{127}Ce [18,19]; ^{128}Ce [20]; ^{129}Ce [19,21]; ^{130}Ce [22]; ^{131}Ce [23]; and ^{132}Ce [24]. In the odd-A cerium isotopes $^{125-131}$Ce, the yrast bands are based upon an $h_{11/2}$ neutron orbital, and several other rotational bands, based on $d_{5/2}$, $g_{7/2}$, and $d_{3/2}$ neutron orbitals, are also observed for each nucleus. In the most neutron deficient of these isotopes, ^{125}Ce, four rotational bands are observed which extend to a maximum spin of $75/2\,\hbar$ [4]. Prior to the present work, very little spectroscopic information was available about ^{123}Ce. No excited states had been observed, but the ground state had been identified using the ^{92}Mo(^{36}Ar,αn) reaction [25]; the ground state was shown to decay by β-delayed proton emission, $^{123}_{58}$Ce$\rightarrow^{123}_{57}$La$\rightarrow^{122}_{56}$Ba, which ultimately populated the 0^+, 2^+, 4^+, and 6^+ states in $^{122}_{56}$Ba. An examination of the proton-decay branches to the ^{122}Ba states led to the assignment of a spin of $5/2$ to the ground state of ^{123}Ce.

The cerium isotopes with $A < 124$ have not been well studied because they are difficult to produce in experiments. The best way to produce them is to use fusion-evaporation reactions, but the isotopes with $A < 126$ can only be reached by neutron evaporation from compound nuclei which are themselves already very neutron deficient. As a result, charged-particle evaporation dominates the total cross section, and cross sections for neutron-evaporation channels are small (often a few μb). Despite this obstacle, such nuclei can be studied if sensitive channel-selection methods are used, as in the present work.

III. EXPERIMENTAL DETAILS

The results presented here were obtained from an experiment carried out using the Argonne Tandem Linac Accelerator System (ATLAS) at Argonne National Laboratory. The experimental details have been described in Refs. [14,26–28]. Excited states in ^{123}Ce were populated using the ^{64}Zn(^{64}Zn,αn) reaction, for which the cross section is predicted by the statistical-model code ALICE [29] to be $\sim$100 μb. The beam of ^{64}Zn ions from ATLAS, with energy 260 MeV and intensity 2 pnA, was incident on a target consisting of a 500-μg/cm^2 ^{64}Zn foil. The target was placed at the center of the Gammasphere γ-ray spectrometer [8], which was used to detect prompt de-excitation γ rays, emitted following fusion-evaporation. When complete, Gammasphere consists of 110 75%-efficient, high-purity, germanium detectors, arranged in 17 rings of constant polar angle, θ. In the present work, the five forwardmost rings of detectors were removed in order to accommodate the Washington University Neutron Shell, and in addition two detectors in the ring at $\theta = 90.0^\circ$ were missing, leaving 78 germanium detectors. The Neutron Shell [11], consisting of 30 BC501A scintillators, was used to detect evaporated neutrons. The Microball charged-particle spectrometer [9] was used to detect evaporated α particles and protons. The Microball consists of 95 CsI(Tl) scintillators, and is sufficiently compact to fit inside the Gammasphere target chamber, surrounding the target. On exiting the Gammasphere target chamber, the recoiling reaction products were dispersed according to their mass-to-charge state (M/q) ratio by the Argonne Fragment Mass Analyzer (FMA) [13] and were detected in a parallel-plate gridded-anode avalanche counter (PGAC) at the focal plane. During the experiment, three different trigger conditions were used: $\gamma\gamma\gamma$ (Gammasphere only); $\gamma\gamma$-neutron (Neutron Shell); or $\gamma\gamma$-recoil (FMA focal-plane PGAC). The experiment was conducted for about 84 h, during which 1.04×10^9 events were collected.

IV. DATA ANALYSIS

A. Detection of evaporated particles

Discrimination between α particles and protons in the Microball was carried out using the methods described in Ref. [9]. In brief, three parameters associated with each Microball signal were recorded: (i) the energy, integrated over the first microsecond of the pulse; (ii) the energy in the tail, integrated over 10 ns, starting 9 μs after the start of the pulse; and (iii) the time between the RF signal of ATLAS and the pulse. By plotting various combinations of these three parameters, excellent separation of protons and α particles was achieved. Detection efficiencies were found to be 84% for protons and 69% for α particles. Similarly, discrimination between γ rays and neutrons in the Neutron Shell was carried out using the methods described in Ref. [11]. A single number defining the detection efficiency for neutrons was not easy to determine for several reasons. First, one of the three triggers used in the experiment included the detection of a neutron ($\gamma\gamma$-neutron), and the data were accordingly biased. Second, the detection efficiency depends on the energy of the evaporated neutron and is, therefore, dependent upon the reaction channel, as discussed in Ref. [11]. Third, a significant proportion of neutrons is observed to scatter between detectors. This has the effect of reducing the neutron-detection efficiency and of "contaminating" gated spectra with γ rays from channels of lower neutron multiplicity. In order to reduce such degradation of the spectra, a method of nearest-neighbor suppression was used as described in Refs. [11,26,30]. This suppression affected the single-neutron detection efficiency ε_n, and also meant that the efficiency for the detection of two neutrons ε_{2n} was not simply ε_n^2. Ultimately, *effective* efficiencies of $\varepsilon_n \simeq 55\%$ and $\varepsilon_{2n} \simeq 9\%$ were obtained.

B. γ-ray spectra

The coincidence data had a mean suppressed γ-ray fold of 2.8. Most of the offline analysis was carried out with twofold

and threefold γ-ray coincidence events. A total of 7.0×10^9 twofold and and 2.7×10^9 threefold events were recorded (after unfolding). Spectra were analyzed using the data-analysis codes GF3, ESCL8R, LEVIT8R [31,32], and DATA_VIEW [33]. Analysis of an ungated $\gamma\gamma\gamma$ cube revealed that excited states were populated in at least 20 evaporation residues, with the most intense being ^{125}La ($3p$), ^{122}Ba ($\alpha 2p$), and ^{124}Ba ($4p$), which constituted 26, 21, and 10% of the data, respectively. In addition to the ungated spectra, $\gamma\gamma$ matrices were created which were gated on all combinations of particles that were likely to be evaporated during the reaction and on different M/q values.

C. Assignment of excited states to ^{123}Ce

It was expected *a priori* that the αn-gated matrix would contain γ rays not only from the αn evaporation channel but also from nuclei produced via the evaporation of αn plus one or more other particles, where the other particles have gone undetected ("$\alpha n+$" channels). It was found that the αn-gated matrix was predominantly composed of γ rays from the αpn channel ^{122}La [26,30] and the $2\alpha n$ channel ^{119}Ba [34], where the proton and second α particle, respectively, had escaped detection. In addition, γ rays belonging to the $\alpha 2n$ evaporation channel, ^{122}Ce, were also observed, but with very low intensity due to the small cross section for that reaction channel. Similarly, γ rays in the $\alpha 2pn$ channel, ^{121}Ba [36], were observed with low intensity, due to the small $\alpha 2pn$ cross section and also due to the low probability of missing both protons with the Microball (2.5%). Thus, the presence of γ rays in the αn-gated matrix does not necessarily mean that they belong to the αn evaporation channel. In order to enhance the relative amount of true αn transitions, fractions of the matrices gated on αpn, $\alpha 2n$, and $2\alpha n$ were subtracted from the αn-gated matrix; this is illustrated in Fig. 1 where Panels (a)–(d) provide the total projections of the matrices gated on αn, αpn, $\alpha 2n$, and $2\alpha n$, respectively. Subtraction of the αpn, $\alpha 2n$, and $2\alpha n$ matrices subtracts γ rays not only from the αpn, $\alpha 2n$, and $2\alpha n$ evaporation channels but also from any channels which are present in these matrices. For example, although a fraction of the $\alpha 2pn$-gated matrix is not subtracted here, γ rays from the $\alpha 2pn$ channel (^{121}Ba) are prominent in the αpn gated matrix, due to one proton going undetected, and are therefore removed from the αn-gated matrix when the αpn-gated matrix is subtracted. Peaks corresponding to transitions in ^{122}La (αpn evaporation), ^{122}Ce ($\alpha 2n$), and ^{119}Ba ($2\alpha n$) are marked in Panels (b)–(d); these transitions are clearly also the most intense in Panel (a). Transitions in ^{122}La (αpn evaporation) are present in the $\alpha 2n$-gated matrix due to scattering between neutron detectors and to the evaporated proton going undetected together with the simultaneous misidentification of a γ ray as a neutron; it should be noted however that there are only $\sim$1% of the counts from the αpn channel in the $\alpha 2n$-gated matrix. In the figure, the positions of the candidate ^{123}Ce transitions are marked by vertical dashed lines: small peaks can be seen in Panel (a) which are not present in Panels (b)–(d). Panel (e) displays the αn-gated matrix projection with suitable fractions of the αpn, αn, and $2\alpha n$ projections subtracted. The spectrum in Panel (e) is of rather poor quality: the negative peaks are due to oversubtraction of transitions present in the $\alpha n+$ matrices, and the broad peaks (below about 300 keV) are γ-ray transitions in the products of the reactions between the ^{64}Zn beam and ^{12}C, built up on the target, or ^{16}O, due to target oxidization; these γ rays have been Doppler corrected with an inappropriate recoil velocity [27]. Despite these issues, the peaks corresponding to the candidate ^{123}Ce transitions are clearly enhanced in Panel (e) compared to Panel (a).

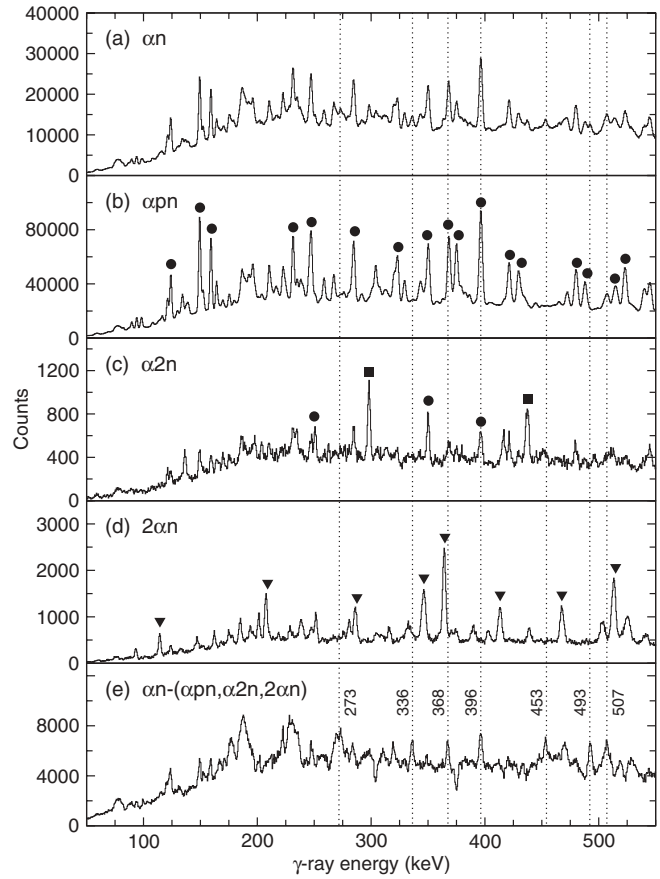

FIG. 1. Projections of $\gamma\gamma$ coincidence matrices, gated on different combinations of evaporated particles, used in the assignment of γ-ray transitions to ^{123}Ce. The spectra shown in Panels (a)–(d) are projections of matrices gated on αn, αpn, $\alpha 2n$, and $2\alpha n$, respectively. The spectrum in Panel (e) is the αn-gated matrix projection with fractions of the αpn, $\alpha 2n$, and $2\alpha n$ projections subtracted, in order to accentuate the peaks belonging to the αn channel (^{123}Ce). Peaks marked with circles, squares, and triangles correspond to transitions in ^{122}La (αpn evaporation), ^{122}Ce ($\alpha 2n$), and ^{119}Ba ($2\alpha n$), respectively. The broad peaks in Panel (e) arise from reactions of the ^{64}Zn beam on ^{12}C or ^{16}O on the target; the width of the peaks is due to the larger Doppler shift due to the larger recoil velocity. Peaks which are enhanced in Panel (e) relative to Panel (a) are assigned to ^{123}Ce; their energies are given in Panel (e), and their positions are marked on all panels by vertical dotted lines.

Using this method, three rotational sequences of transitions were observed. The most intense sequence, referred to as Band 1, was observed by gating on γ-ray energy 336 keV. The second most intense sequence, Band 2, was observed by gating

on 273 keV, and the third, Band 3, was observed by gating on 493 keV. Although the evidence from charged-particle selection suggests that these bands belong to ^{123}Ce, further confirmation is required before a firm assignment can be made. The γ rays in the αn-gated matrix could belong to an $\alpha n+$ channel, in which case they would also be present in at least one of the matrices gated on αn plus one extra particle: specifically, $\alpha 2n$, αpn, or $2\alpha n$. Gating on these matrices did not reveal any evidence for the candidate transitions, supporting the assignment to the αn evaporation channel.

Another consequence of the fact that one or more of the evaporated particles can escape detection is that γ rays belonging to the αn channel will also be present in the matrices gated on the α and n evaporation channels and in the matrix incremented when nothing is detected in the Microball or Neutron Shell (0-gated). Furthermore, using the measured particle-detection efficiencies, it is possible to estimate the expected intensities of the αn γ rays in each of these matrices. Although the candidate ^{123}Ce γ rays appeared to be present in the n- and 0-gated matrices, contaminants from other more intense reaction channels meant that it was not possible to make a meaningful measurement of their intensities. It was, however, possible to measure their intensities in the αn-[$I(\alpha n)$] and α-gated [$I(\alpha)$] matrices. The ratios of these intensities, $I(\alpha)/I(\alpha n)$, are given in Fig. 2 for the three candidate ^{123}Ce bands in comparison to transitions in other bands present in both of the matrices.

A consideration of particle-detection efficiencies reveals that γ rays from all evaporation channels in which *at least* one α particle is emitted, and *exactly* one neutron ($1n$ channels), will have the same value of the intensity ratio $I(\alpha)/I(\alpha n)$, given by $(1-\varepsilon_n)/\varepsilon_n$. Similarly, γ rays from evaporation channels in which at least one α particle is emitted and exactly *two* neutrons ($2n$ channels) will have a ratio of $(1-\varepsilon_n)/2\varepsilon_n$. With $\varepsilon_n = 0.5$, the ratio $I(\alpha)/I(\alpha n)$ would have values of 1.0 for $1n$ channels and 0.5 for $2n$ channels. On Fig. 2, the ratios for the candidate ^{123}Ce bands have a weighted average of 1.17(7). This value is similar to those for bands in ^{122}La (αpn evaporation) and ^{119}Ba ($2\alpha n$ evaporation) which are 1.08(5) and 1.00(14), respectively. The values for ^{122}Ce ($\alpha 2n$ evaporation) and ^{121}La ($\alpha p2n$ evaporation) are 0.52(6) and 0.49(7), respectively. The values for the channels involving the same number of evaporated neutrons differ slightly; this is presumably due to the energy dependence of the neutron-detection efficiency, as discussed in Ref. [11], and also to differing γ-ray multiplicities. The results clearly show that the candidate ^{123}Ce bands are produced in a one-neutron evaporation channel and therefore support the assignment of the bands to ^{123}Ce. The large range of recoil angles associated with α-particle-evaporation channels meant that the transport efficiency of the FMA for these residues was found to be about 2%. Thus, it was not possible to use the FMA data for α-particle evaporation channels with low cross sections, such as ^{123}Ce.

Together, all of the data strongly support the assignment of excited states to ^{123}Ce. Once this assignment had been made, the objective of the analysis changed to obtaining the best possible γ-ray spectra, in order to determine the arrangement of excited states. An αn-gated cube was constructed, but the intensity of the ^{123}Ce transitions within the cube was very low, presumably due to the low γ-ray fold in this weakly populated reaction channel. The α-, n-, and 0-gated matrices were found to be significantly contaminated with transitions from other reaction products. The spectra with the best peak-to-background ratio for the ^{123}Ce transitions were obtained from the matrix gated on αn only. Representative spectra from the αn-gated matrix, showing the bands assigned to ^{123}Ce, are presented in Fig. 3: Bands 1, 2, and 3 are given in Panels (a), (b), and (c), respectively.

D. Angular-intensity ratios

Angular-intensity measurements were carried out in order to help determine multipolarities of the transitions, and, hence, assign relative spins and parities to the excited states. Due to the low intensity of the ^{123}Ce channel, angular-distribution measurements using data from each ring of Gammasphere were not possible. However, indications of transition multipolarities were obtained by comparing the ratios of intensities of γ rays emitted at angles close to and perpendicular to the direction of the beam. As such, intensities at polar angles in the range $79 \leqslant \theta \leqslant 101^\circ$ ($\theta \approx 90^\circ$) were compared to intensities at $129 \leqslant \theta \leqslant 149^\circ$ ($\theta \approx 140^\circ$). The intensities were measured by constructing two $\gamma\gamma$ matrices, which were incremented

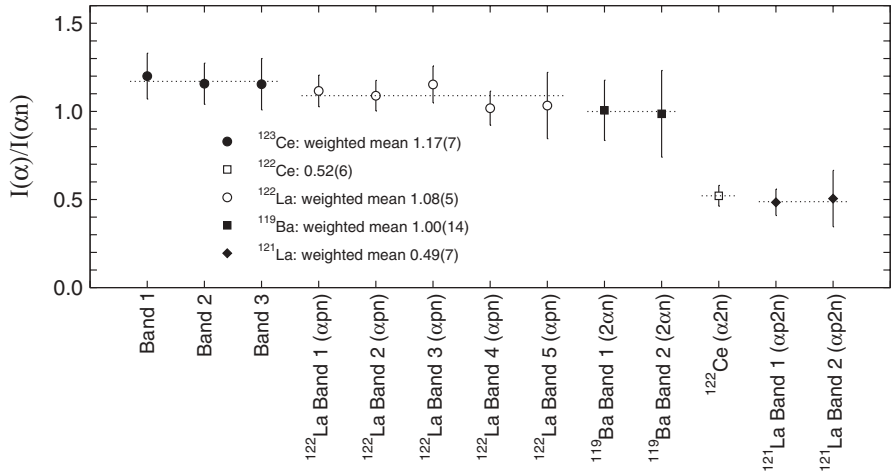

FIG. 2. Ratios of intensities of γ-ray transitions in the α- and αn-gated matrices. Data are given for the three bands assigned to ^{123}Ce, in comparison to bands in ^{122}La (αpn evaporation) [26,30], ^{119}Ba ($2\alpha n$) [34], ^{122}Ce ($\alpha 2n$) [14], and ^{121}La ($\alpha p2n$) [35]. The ratios for the three bands assigned to ^{123}Ce are close to the values for the other single-neutron evaporation channels (αpn and $2\alpha n$) and are distinctly different from the two-neutron-evaporation channels ($\alpha 2n$ and $\alpha p2n$).

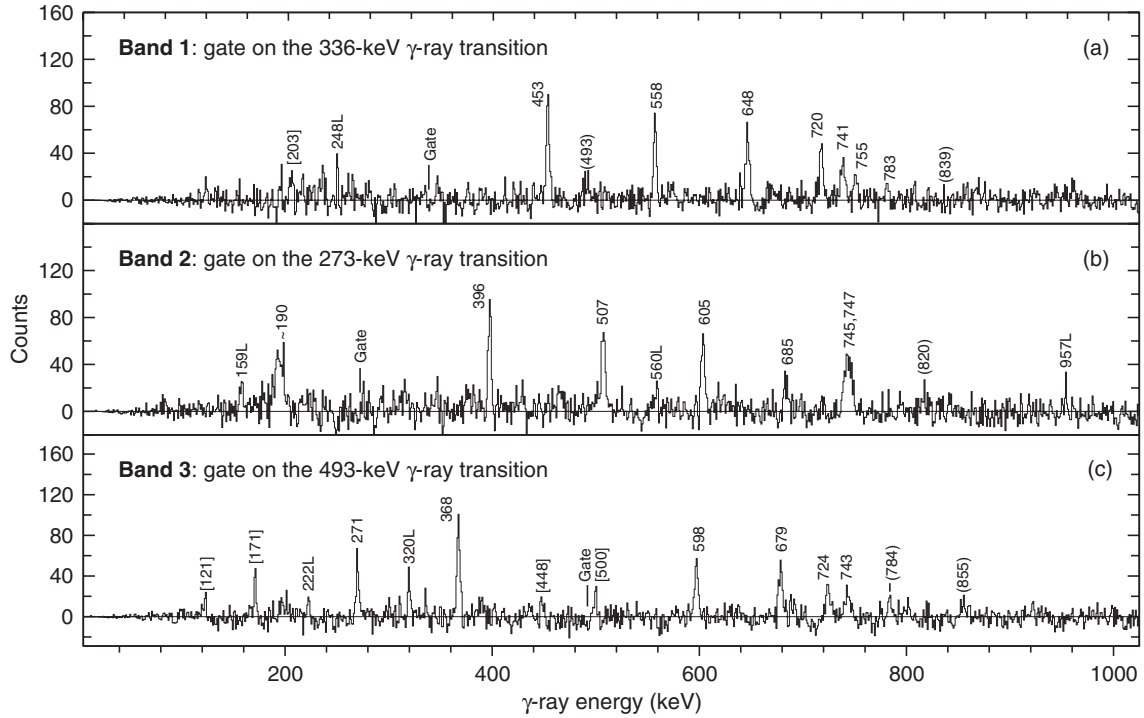

FIG. 3. γ-ray spectra projected from the αn-gated matrix, showing the three rotational bands assigned to ^{123}Ce. The spectra were gated on the 336-, 273-, and 493-keV transitions, as indicated in the panels. Tentative transitions have labels in parentheses. The transitions with labels succeeded by the letter L belong to ^{122}La, and the large peak at ∼190 keV in Panel (b) is from the ^{12}C(^{64}Zn,pn)^{74}Br reaction, due to carbon buildup on the target [27]. The transitions with labels in square brackets at energies 121, 171, 203, 448, and 500 keV appear to be in coincidence with the ^{123}Ce bands but could not be placed in the level scheme.

with γ-ray energies from all germanium detectors (all θ values) on one axis, and with γ-ray energies from detectors at a particular value of θ on the other axis. These matrices were gated on the αn evaporation channel; although gating on the α channel (in addition to αn) would have increased the intensities of the αn γ rays in the matrices, it also significantly increased intense contaminants such as ^{123}La (αp evaporation) and ^{122}Ba ($\alpha 2p$). By gating on the "all" germanium-detector axis of each matrix, the intensity of a γ ray at a particular θ could be measured. Using this method, γ-ray intensities at $\theta \simeq 140$ and $\simeq 90^\circ$ were measured, and the ratio R of these values $I(\sim 140^\circ)/I(\sim 90^\circ)$ was taken. After correcting for detection efficiencies, R was found to be near 0.7 for a stretched-dipole transition and near 1.2 for a stretched-quadrupole transition. These values were calibrated using transitions in ^{122}La [26,30] which was produced in the αpn evaporation channel and which was present with significant intensity in the αn-gated matrices.

V. RESULTS

The level scheme of ^{123}Ce deduced in this work is presented in Fig. 4. The excited states form three rotational bands, labeled Band 1, Band 2, and Band 3. The properties of the γ-ray transitions are given in Table I. The spins and parities assigned to the lowest states in each band are proposed by comparison to the level structures of neighboring nuclei (discussed later); relative to the lowest states, spins and parities have been assigned with the help of the measured angular-intensity ratios, R. For these reasons, all of the spins and parities in Fig. 4 are tentative. The level energies are given in Fig. 4 relative to the lowest state in each of the respective bands; the excitation energies will, therefore, be subject to different energy offsets. It should perhaps be noted that transitions at 396.4 and 507.2 keV have been assigned to ^{123}Ce, while there are transitions at 395.1 and 507.8 keV decaying from excited states of ^{122}La (produced here via αpn evaporation). Despite the similarity in energies, coincidence relationships firmly establish that these are different transitions. Indeed, the 396- and 507-keV transitions assigned to ^{123}Ce are mutually coincident, whereas the transitions with similar energies in ^{122}La are not.

The angular-intensity ratios were measured for all but six of the transitions; the low-intensity and tentative transitions could not be measured. All of the transitions in Fig. 4 have values consistent with a stretched-quadrupole character and have, therefore, been assigned as stretched-$E2$ transitions. In Band 2, the 273-keV transition has an angular-intensity ratio which is consistent with either $\Delta I = 2$ or 1, but which is closer to $\Delta I = 1$. On the basis of excitation-energy systematics, however, this transition has been assigned to be of $E2$ character and to be a member of the rotational band. The angular-intensity ratio of the 273-keV transition can perhaps be explained by fusion-evaporation reactions between the ^{64}Zn beam and target contaminants ^{12}C or ^{16}O, as mentioned earlier. One such reaction product is ^{74}Br, produced via the ^{12}C(^{64}Zn,pn) or ^{16}O(^{64}Zn,αpn) reaction; the broad peak at 273 keV apparent in Fig. 1(e) is due to the $7^+ \rightarrow 6^+$ $M1/E2$

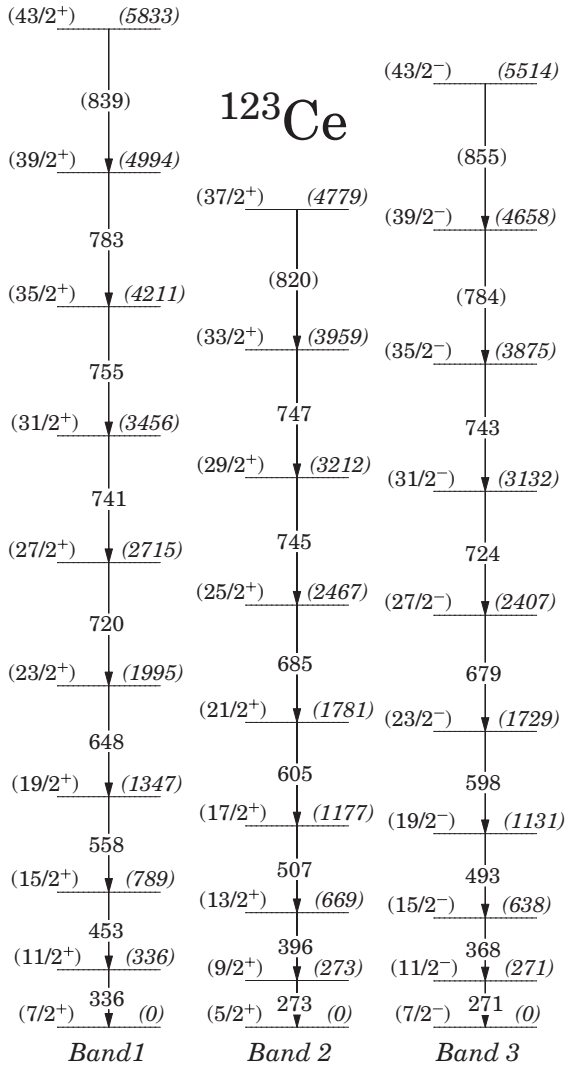

FIG. 4. The rotational bands assigned to ^{123}Ce in this work. The spins and parities of the states have been assigned tentatively, as described in the text. The transitions with energies in parentheses have been tentatively placed. The level energies are given relative to the lowest state in each band.

transition in ^{74}Br [37]. This assignment has been confirmed by coincidence relationships with other transitions in ^{74}Br and is discussed in more detail in Ref. [27]. It should also be noted that the angular-intensity ratios for Bands 1 and 3 exhibit a wide variation. The reason for this observation is not clear. However, most of the transitions in Band 3 could only be clearly measured in a spectrum gated on the 493-keV transition, which overlaps with the Doppler-corrected 511-keV γ rays from e^+e^- annihilation; this will introduce random coincidences.

Given the spin assignments in Fig. 4, Band 1 consists of nine $E2$ transitions, extending from the $(7/2^+)$ state to the $(43/2^+)$ state at 5.833 MeV, Band 2 consists of eight $E2$ transitions, extending from the $(5/2^+)$ state to the $(37/2^+)$ state at 4.779 MeV, and Band 3 consists of nine transitions, extending from the $(7/2^-)$ state to the $(43/2^-)$ state at 5.514 MeV. The bands are populated to high spins with reasonably constant intensity, which only decreases significantly over the highest two or three states. Several transitions were identified which appeared to be in coincidence with the bands assigned to ^{123}Ce, but which could not be placed in the level scheme. Some of these transitions (121, 171, 203, 448, and 500 keV) are apparent in the spectra of Fig. 3. It is possible that some of these correspond to $M1/E2$ interband transitions between the bands, as discussed in Sec. VI C. However, there is no choice of energy offset for any of the bands which can reproduce energy differences between states corresponding to more than one of these transition energies.

The aligned angular momenta of the bands have been calculated using the method described in Ref. [38] assuming the spins assigned in Fig. 4 and are plotted against rotational frequency in Fig. 5. The K values used are given and discussed in Sec. VI. A reference with Harris parameters [39] of $\mathcal{J}_0 = 26.2\ \mathrm{MeV}^{-1}\hbar^2$ and $\mathcal{J}_1 = 17.5\ \mathrm{MeV}^{-3}\hbar^4$ has been subtracted from all of the data points. These Harris parameters were obtained from a fit to the ground-state band in the even-even core, ^{122}Ce [14]. The aligned angular momenta are discussed in Sec. VI D.

VI. DISCUSSION

In order to help identify the orbitals underlying the ^{123}Ce bands, total Routhian surface (TRS) and cranked shell-model (CSM) calculations were carried out. The TRS calculations were used to predict the deformations associated with the likely single-neutron configurations, and these deformations were, in turn, used as input into CSM calculations, which predicted the properties of rotational alignments. The experimental aligned angular momenta were compared to the theoretical predictions for different configurations. It is proposed that Bands 1 and 2 are likely to be based on the $\nu(g_{7/2})[413]5/2^+$ orbital, and Band 3 is likely to be based on the $\nu(h_{11/2})[532]5/2^-$ orbital. The reasons for these assignments are discussed in the following sections.

A. Total Routhian surface calculations

The TRS method is described in detail in Refs. [40–43]. In essence, for a given number of quasiparticles with specific parity (π) and signature (α), the total Routhian of the nucleus is minimized with respect to the deformation parameters β_2, β_4, and γ, at specified steps in rotational frequency, resulting in a "total Routhian surface" for that frequency. Although each TRS has a well-defined parity and signature, no other quantum numbers are conserved. The likely single-neutron configurations in ^{123}Ce were determined by calculating [44] the ordering of single-particle orbitals in a Woods-Saxon potential at $\beta_2 = 0.3$ (the approximate deformations of configurations in ^{125}Ce [4]), and also by considering the known configurations in neighboring nuclei, such as ^{122,124,125}Ce [4,14], ^{122}La [26,30], and ^{121}Ba [36]. The deformations of the configurations expected in ^{123}Ce were then extracted from the TRS calculations. The standard nomenclature for labeling orbitals has been adopted, which is summarized in Table II. The positive-parity orbitals have been labeled with the spherical

TABLE I. Properties of the γ rays assigned to the decay of excited states in ^{123}Ce. The E_γ values are the γ-ray energies in keV, and I_γ are the γ-ray intensities. The R values are the angular-intensity ratios, as discussed in the text. The lowest four rows give transitions in ^{122}La which were used to calibrate the values of R.

E_γ (keV)	I_γ	R	ΔI	$I_i^{\pi_i} \rightarrow I_f^{\pi_f}$	Multipolarity
			Band 1		
335.8(1)	89(4)	1.1(2)	2	$11/2^+ \rightarrow 7/2^+$	$E2$
453.1(1)	100(4)	1.2(3)	2	$15/2^+ \rightarrow 11/2^+$	$E2$
558.2(1)	94(4)	1.3(2)	2	$19/2^+ \rightarrow 15/2^+$	$E2$
648.1(1)	94(5)	1.2(2)	2	$23/2^+ \rightarrow 19/2^+$	$E2$
719.9(1)	86(4)	1.5(3)	2	$27/2^+ \rightarrow 23/2^+$	$E2$
741.0(2)	85(4)	1.5(4)	2	$31/2^+ \rightarrow 27/2^+$	$E2$
754.6(2)	80(4)	1.6(4)	2	$35/2^+ \rightarrow 31/2^+$	$E2$
783.4(2)	68(3)	1.6(6)	2	$39/2^+ \rightarrow 35/2^+$	$E2$
839(1)	21(4)		2	$43/2^+ \rightarrow 39/2^+$	$E2$
			Band 2		
273.0(1)	94(8)	0.77(16)	2	$9/2^+ \rightarrow 5/2^+$	$E2$
396.4(1)	98(8)	1.3(2)	2	$13/2^+ \rightarrow 9/2^+$	$E2$
507.2(1)	95(9)	1.4(3)	2	$17/2^+ \rightarrow 13/2^+$	$E2$
604.6(1)	94(8)	1.4(3)	2	$21/2^+ \rightarrow 17/2^+$	$E2$
685.4(2)	85(15)	1.1(4)	2	$25/2^+ \rightarrow 21/2^+$	$E2$
745(1)	86(11)		2	$29/2^+ \rightarrow 25/2^+$	$E2$
747(1)	81(11)		2	$33/2^+ \rightarrow 29/2^+$	$E2$
820(1)	51(13)		2	$37/2^+ \rightarrow 33/2^+$	$E2$
			Band 3		
270.7(1)	88(6)	1.1(2)	2	$11/2^- \rightarrow 7/2^-$	$E2$
367.8(1)	88(6)	1.07(12)	2	$15/2^- \rightarrow 11/2^-$	$E2$
492.6(1)	71(11)	0.91(19)	2	$19/2^- \rightarrow 15/2^-$	$E2$
597.5(1)	62(7)	1.00(17)	2	$23/2^- \rightarrow 19/2^-$	$E2$
678.7(1)	41(7)	1.1(3)	2	$27/2^- \rightarrow 23/2^-$	$E2$
724.4(2)	34(8)	1.6(5)	2	$31/2^- \rightarrow 27/2^-$	$E2$
743.2(2)	21(9)	1.7(5)	2	$35/2^- \rightarrow 31/2^-$	$E2$
783.6(2)	13(8)		2	$39/2^- \rightarrow 35/2^-$	$E2$
855(1)	5(2)		2	$43/2^- \rightarrow 39/2^-$	$E2$
			Calibration transitions		
231		1.23(13)	2	^{122}La	$E2$
560		1.22(12)	2	^{122}La	$E2$
149		0.69(7)	1	^{122}La	$M1/E2$
324		0.67(8)	1	^{122}La	$M1/E2$

subshell from which they originate, but at the deformations discussed here they will be strongly mixed. For example, orbitals of $g_{7/2}$ and $d_{5/2}$ parentage will mix and exchange character. The TRS-calculated deformations for the likely single-neutron configurations in ^{123}Ce are given in Table III.

B. Cranked Woods-Saxon calculations

In order to predict details of quasiparticle alignments for different neutron configurations, cranked shell-model (CSM) calculations have been performed using a Woods-Saxon potential [44,45]. In the calculations, the pairing strength was calculated at zero frequency and decreased with increasing rotational frequency so that it reached 50% of its original value at 0.7 MeV/$\hbar$ [42]. The TRS calculations (Table III) reveal that the likely single-neutron configurations in ^{123}Ce have a slight variation in deformation. In order to investigate how the calculated alignment frequencies depend on the deformation, CSM calculations have been carried out where one of the three deformation parameters, β_2, β_4, and γ, has been varied while the other two are kept fixed. The results of this investigation are given in Fig. 6; the ranges of deformations given in Table III [$0.293 \leqslant \beta_2 \leqslant 0.320, 0.028 \leqslant \beta_4 \leqslant 0.043$, $-4.1 \leqslant \gamma \leqslant 0.4^\circ$] are bounded by the vertical dashed lines in each panel. Over these ranges of deformations there is very little change in any of the calculated alignment frequencies. For this reason, the alignment frequencies calculated at a representative deformation of $\beta_2 = 0.3, \beta_4 = 0.03, \gamma = 0^\circ$ are applicable to bands built on all of the neutron orbitals listed in Table III. These calculated alignment frequencies are given in Table IV.

C. Configuration assignments

Inspection of the aligned angular momenta of the bands in ^{123}Ce (Fig. 5) reveals that Bands 1 and 2 have identical behavior, given the spin assignments in Fig. 4. Furthermore, these bands are populated with very similar intensities. These

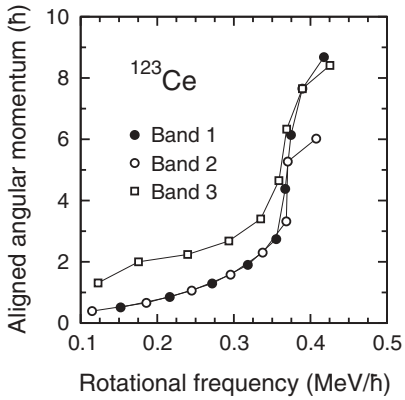

FIG. 5. Aligned angular momenta of the bands assigned to ^{123}Ce. For all data points, a reference with Harris parameters of $\mathcal{J}_0 = 26.2\ \mathrm{MeV}^{-1}\hbar^2$ and $\mathcal{J}_1 = 17.5\ \mathrm{MeV}^{-3}\hbar^4$ has been subtracted.

observations suggest that Bands 1 and 2 are signature partners with small or zero signature splitting. If the bands were based on a negative-parity $h_{11/2}$ neutron, it would be expected that they would have nonzero signature splitting due to the position of the Fermi level at $N = 65$. It is, therefore, likely that Bands 1 and 2 are based on a positive-parity $d_{5/2}$ or $g_{7/2}$ neutron.

Studies of the neighboring odd-A ^{125,127,129}Ce isotopes [4,15,16,18,19,21] have identified bands based on $\nu(h_{11/2})$, $\nu(g_{7/2})$, and $\nu(d_{5/2})$ orbitals. Although the most intensely populated positive-parity band in ^{125}Ce has previously been assigned to have the $\nu(d_{5/2})[402]5/2^+$ configuration [4,15,16], this assignment has been drawn into question by the recent study of ^{127}Ce in Ref. [19], where it has been established that the ground state of ^{127}Ce is based on a neutron in a $\nu(d_{3/2})[411]1/2^+$ orbital. This suggests that at $N = 69$ (^{127}Ce) the neutron Fermi level already lies below the $\nu(d_{5/2})[402]5/2^+$ orbital. This would then imply that for ^{125}Ce ($N = 67$) the most intense positive-parity band could be assigned to the $\nu(g_{7/2})[413]5/2^+$ orbital. In support of this argument, a low-lying isomeric state with spin $1/2$ was recently identified in ^{125}Ce [46] which could correspond to the bandhead of the $\nu(d_{3/2})[411]1/2^+$ sequence. It would be consistent with these arguments to assign a configuration of $\nu(g_{7/2})[413]5/2^+$ to Bands 1 and 2 in ^{123}Ce.

TABLE II. Nomenclature for orbitals near the Fermi surface in ^{123}Ce, with $\beta_2 = 0.3$.

	Nilsson configuration		Label	
	Subshell	$[Nn_z\Lambda]\Omega^\pi$	$\alpha = -1/2$	$\alpha = +1/2$
Neutrons	$g_{7/2}$	$[413]5/2^+$	B	A
	$d_{5/2}$	$[411]3/2^+$	C	D
	$h_{11/2}$	$[532]5/2^-$	E	F
	$h_{11/2}$	$[523]7/2^-$	G	H
Protons	$g_{9/2}$	$[404]9/2^+$	b	a
	$d_{5/2}$	$[411]3/2^+$	d	c
	$h_{11/2}$	$[550]1/2^-$	e	f
	$h_{11/2}$	$[541]3/2^-$	g	h

TABLE III. Deformations of configurations based on different neutron orbitals in ^{123}Ce. The left-hand column $\nu(\pi,\alpha)$ gives the orbital of the neutron in the standard nomenclature, together with its signature (α) and parity (π) quantum numbers. The other three columns give the β_2, γ, and β_4 deformation parameters as calculated by TRS calculations at a rotational frequency of $\omega = 0.187$ MeV/$\hbar$.

$\nu(\pi,\alpha)$	β_2	γ	β_4
A(+, +1/2)	0.305	−2.1°	0.033
B(+, −1/2)	0.305	−0.6°	0.033
C(+, −1/2)	0.307	+0.4°	0.037
D(+, +1/2)	0.305	−0.9°	0.035
E(−, −1/2)	0.293	−2.6°	0.028
F(−, +1/2)	0.294	−1.5°	0.028
G(−, −1/2)	0.298	−4.1°	0.028
H(−, +1/2)	0.320	−1.1°	0.043

If Bands 1 and 2 are signature partners, then it would perhaps be surprising that no interband transitions are observed, even at low spins. To investigate this nonobservation, the ratios of reduced transition probabilities $B(M1; I \to I-1)/B(E2; I \to I-2)$ have been calculated for the band based upon the $\nu(g_{7/2})[413]5/2^+$ orbital, using the methods described in Ref. [4]. To calculate $B(M1; I \to I-1)/B(E2; I \to I-2)$ ratios it is necessary to know the value of the orbital gyromagnetic factor g_K: here, the Schmidt value of $g_K = 0.26$ has been assumed. Over the spin range 7/2 to 43/2, the $B(M1)/B(E2)$ ratio has values <0.03 $(\mu_N/e\mathrm{b})^2$. Assuming no signature splitting (as in ^{125}Ce [4]) these $B(M1; I \to I-1)/B(E2; I \to I-2)$ values suggest that the intensities of any $M1/E2$ interband transitions between Bands 1 and 2 will be $<2\%$ of the intensities of in-band $E2$ transitions. However, in the neighboring isotope ^{125}Ce [4], measured $B(M1)/B(E2)$ values in the analogous band are significantly larger than would be expected for the $\nu(g_{7/2})[413]5/2^+$ configuration, with $M1/E2$ interband transitions having intensities of around 50% of the in-band $E2$ transitions at low spins. This observation, although seemingly contradictory to the configuration assignments proposed here, could perhaps be explained by mixing between close-lying $\nu(g_{7/2})$ and $\nu(d_{5/2})$ positive-parity orbitals. If this were also the case in ^{123}Ce, then it should be possible to observe the most intense interband transitions. There are several candidate interband transitions in the spectra, such as the 203-keV transition in Fig. 3, but it has not been possible to place these transitions in the level scheme with any confidence. It is perhaps worth noting that structures based on the $\nu(g_{7/2})[413]5/2^+$ orbital have been observed in the isotone ^{121}Ba [47] and in the neighboring nuclei ^{119}Ba [34] and ^{119}Xe [48]. In these structures, some weak interband transitions are observed at low spins.

In the neighboring ^{125,127,129}Ce nuclei, one of the most intensely populated bands is based on a $\nu(h_{11/2})$ orbital. For this reason, and from the excitation-energy systematics discussed below, in the present work Band 3 has been assigned to have the $\nu(h_{11/2})[532]5/2^-$ configuration. Calculations suggest that in the neutron-deficient cerium isotopes ($A \lesssim 132$), the quadrupole deformation will increase as the neutron number decreases. This is illustrated in Fig. 7 where the

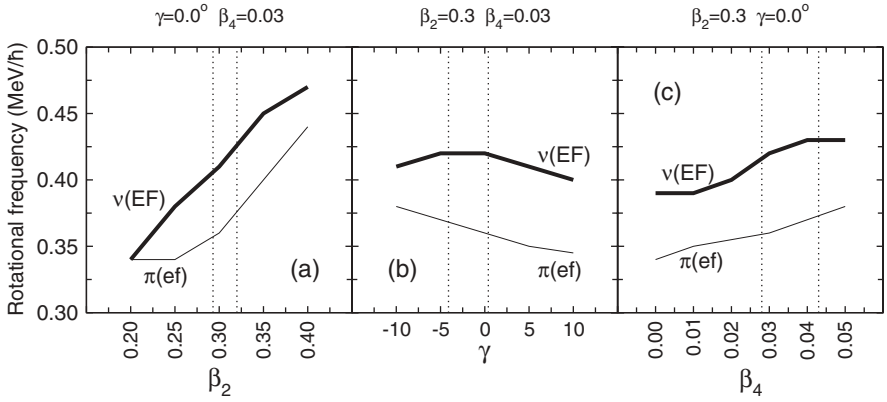

FIG. 6. Frequencies of the lowest neutron (EF) and proton (ef) $(h_{11/2})^2$ quasiparticle alignments for ^{123}Ce, extracted from cranked shell-model calculations. The neutron and proton alignments are shown by thick and thin solid lines, respectively. The vertical dotted lines mark the ranges of deformations of the likely single-neutron configurations (Table III). Apart from the parameter being varied, the deformations are fixed at $\beta_2 = 0.3$, $\gamma = 0.0^\circ$, and $\beta_4 = 0.03$.

calculated quadrupole deformation parameters β_2 are presented for odd-A cerium isotopes with mass numbers $119 \leqslant A \leqslant 133$. The predictions in Fig. 7 are taken from the macroscopic-microscopic calculations of Ref. [6] (Möller *et al.*), the self-consistent Hartree-Fock Bogoliubov mean-field calculations of Ref. [7] (Duguet *et al.*), and from the TRS calculations. The TRS results are given for the lowest-lying negative-parity (E) and positive-parity (A) neutron configurations. All of the calculations predict that the deformation in ^{123}Ce will be larger than that of ^{125}Ce.

If the deformation is larger, the moment of inertia is larger as well, and the quadrupole transition energies should be correspondingly lower in ^{123}Ce than in analogous bands in ^{125}Ce. Furthermore, with large deformations of $\beta_2 \simeq 0.30$, it is expected that the transition energies will vary smoothly as a function of neutron number, for bands based on the same underlying configuration. Figure 8 provides the excitation energies of states of $\nu(h_{11/2})$ ($\alpha = -1/2$) bands of ^{125,127,129}Ce relative to the lowest state in each band and compares these with ^{123}Ce Band 3. The latter data are in reasonably good systematic agreement with the neighboring nuclei. The energy separations of states in Band 3 of ^{123}Ce are lower than in the neighboring nuclei, suggesting increasing deformation.

D. Quasiparticle alignments

The aligned angular momenta i_x of the bands have been calculated using the method described in Ref. [38] assuming the spins assigned in Fig. 4 and are plotted against rotational frequency in Fig. 5. A value of $K = 5/2$ was used for each of the bands. A reference, with Harris parameters [39] of $\mathcal{J}_0 = 26.2\ \text{MeV}^{-1}\hbar^2$ and $\mathcal{J}_1 = 17.5\ \text{MeV}^{-3}\hbar^4$, has been subtracted from all of the data points. These Harris parameters were obtained from a fit to the ground-state band of the even-even core ^{122}Ce [14].

All of the bands exhibit similar behavior, with an upbend at 0.36 MeV/$\hbar$. The increase in i_x for each of the bands is about 7 or 8 $\hbar$; the increase is possibly larger for Band 1 than for Bands 2 and 3, although that observation depends solely on tentative transitions. In accordance with Table IV and Fig. 6, the observed upbends are assigned to the alignment of the lowest pair of $h_{11/2}$ protons (ef). The aligned angular momenta of the bands in ^{123}Ce are compared to bands in neighboring nuclei in Fig 9. In all panels of the figure, the bands in ^{123}Ce are shown as thin solid (Band 1), dotted (Band 2), and dashed (Band 3) lines. A reference with the same Harris parameters as in Fig. 5 has been subtracted from all data points. Use of the same Harris parameters for all of the nuclei shown enables a meaningful comparison of their i_x values.

Figure 9(a) provides the i_x values for the $\nu(h_{11/2})[523]7/2^-$ ($\alpha = -1/2$) bands in ^{125,127,129}Ce. In these bands, the backbend at 0.36 MeV/$\hbar$ is assigned to the $\pi(h_{11/2})^2$ (ef) alignment; the $\nu(h_{11/2})^2$ (EF) alignment is blocked. Figure 9(b) shows i_x values for positive-parity bands in ^{125,127,129}Ce. Like the

TABLE IV. Frequencies of alignments of quasiparticle pairs in ^{123}Ce, calculated by the cranked shell model, with $\beta_2 = 0.30$, $\gamma = 0.0^\circ$, and $\beta_4 = 0.03$.

Protons		Neutrons	
Pair	ω (MeV/$\hbar$)	Pair	ω (MeV/$\hbar$)
ef	0.35	EF	0.41
fg	0.50	FG	0.51
eh	0.56	EH	0.60
ab	>0.7	AB	>0.6

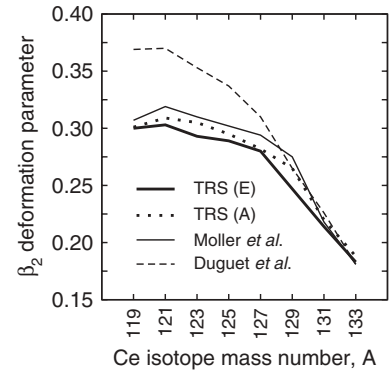

FIG. 7. Calculated quadrupole deformation parameters β_2 of the odd-A cerium ($Z = 58$) isotopes, plotted against mass number A. The total Routhian surface (TRS) calculations were carried out for the lowest negative-parity (E) and positive-parity (A) single-neutron configurations. Also shown are the results of the macroscopic-microscopic calculations by Möller *et al.* [6] and the results of self-consistent Hartree-Fock Bogoliubov mean-field calculations by Duguet *et al.* [7].

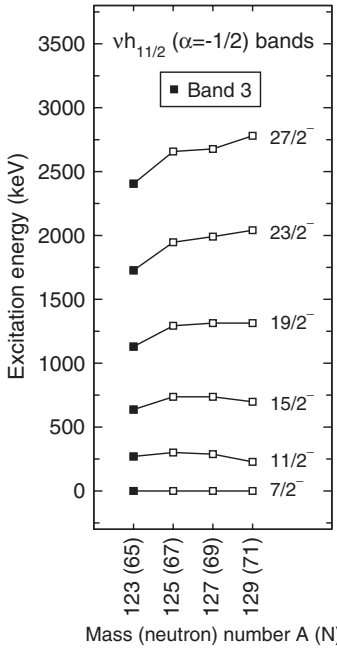

FIG. 8. Excitation energies of the lowest six states in the $\nu(h_{11/2})$ ($\alpha = -1/2$) bands of odd-A ^{125,127,129}Ce isotopes [4,19] compared to states in Band 3 identified in this work. The excitation energies are given relative to the lowest state in each band.

[523]7/2$^-$ bands [Panel (a)], the backbend at 0.36 MeV/$\hbar$ is assigned to the $\pi(h_{11/2})^2$ (ef) alignment. Unlike the [523]7/2$^-$ bands, the $\nu(h_{11/2})^2$ (EF) alignment is not blocked; although there is no sharp upbend or backbend, this EF alignment is thought to be the reason why the values of i_x above ~0.4 MeV/$\hbar$ are larger than in Panel (a). For both Panels (a) and (b), the $\pi(h_{11/2})^2$ alignment at 0.36 MeV/$\hbar$ changes from a clear backbend in ^{129}Ce to an upbend in ^{123}Ce; this is presumably due to the change in interaction strength with neutron number, as predicted by the CSM and discussed in Ref. [4]. Below a rotational frequency of 0.4 MeV/$\hbar$, the behavior of all of the bands in ^{123}Ce is very similar to the bands shown in both Panels (a) and (b), which suggests that the $\pi(h_{11/2})^2$ pair is aligning in ^{123}Ce as well. The ^{123}Ce bands, unfortunately, do not extend to sufficiently high rotational frequencies to determine whether the $\nu(h_{11/2})^2$ alignment takes place. Observation of the $\pi(h_{11/2})^2$ alignments in the bands is consistent with the proposed configurations.

In Fig. 9(c), the aligned angular momentum in the ground-state bands of the even-even neighbors, ^{122,124}Ce, is compared to the bands in ^{123}Ce. Neither the lowest $\pi(h_{11/2})^2$ (ef) nor the $\nu(h_{11/2})^2$ (EF) alignments are blocked in the even-even nuclei. Below 0.4 MeV/$\hbar$, the behavior of the bands in ^{123}Ce is very similar to the even-even neighbors. Figure 9(d) gives the aligned angular momentum of two bands which are built on unpaired $h_{11/2}$ protons: the yrast $\pi(h_{11/2})$ band in ^{123}La and the yrast $\nu(h_{11/2}) \otimes \pi(h_{11/2})$ band in ^{122}La. In both bands, the $\pi(h_{11/2})^2$ (ef) alignment is blocked, and there is clearly no upbend at 0.36 MeV/$\hbar$, in contrast to the bands in ^{123}Ce. The $\nu(h_{11/2})^2$ (EF) alignment is blocked in the ^{122}La band, but is not blocked in the ^{123}La band, and accounts for the slow rise in i_x above 0.4 MeV/$\hbar$.

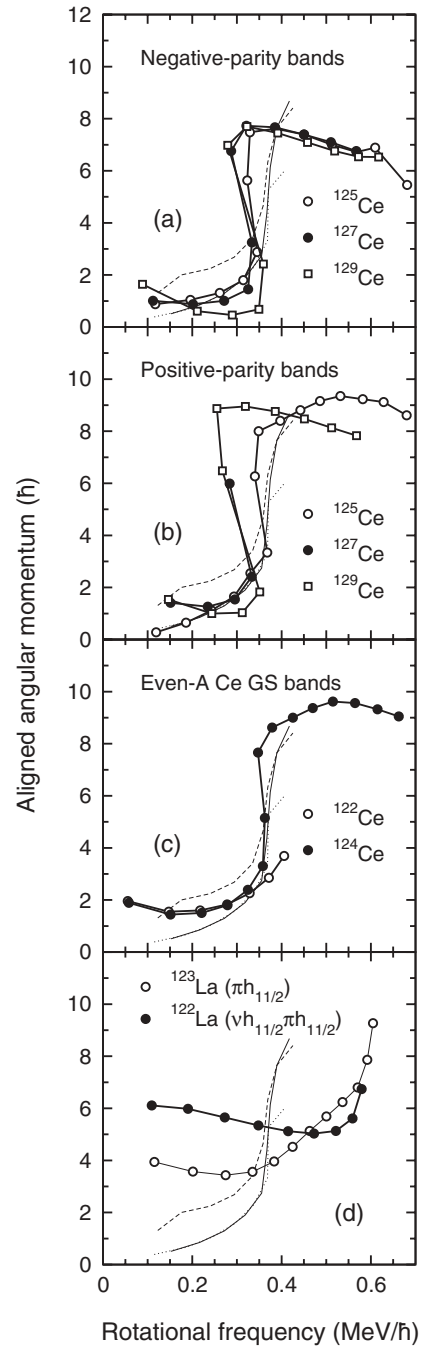

FIG. 9. Aligned angular momenta of nuclei neighboring ^{123}Ce, in comparison with the three bands identified in this work. Bands 1, 2, and 3 of ^{123}Ce are shown in all of the panels by the thin solid, dotted, and dashed lines, respectively. Panel (a) shows the favored signature ($\alpha = -1/2$) of the $\nu(h_{11/2})[523]7/2^-$ bands of ^{125,127,129}Ce, and (b) shows the positive-parity bands [$\nu(d_{5/2})$ and $\nu(g_{7/2})$] in the same nuclei. Panel (c) provides information on the ground-state (GS) bands in the even-even neighbors ^{122,124}Ce. Panel (d) gives data for two bands involving an unpaired $h_{11/2}$ proton: the $\pi(h_{11/2})[550]1/2^-$ ($\alpha = -1/2$) band in ^{123}La and the $\nu(h_{11/2})[532]5/2^- \otimes \pi(h_{11/2})[550]1/2^-$ ($\alpha = 0$) band in ^{122}La. For all data points, a reference with Harris parameters of $\mathcal{J}_0 = 26.2$ MeV$^{-1}\hbar^2$ and $\mathcal{J}_1 = 17.5$ MeV$^{-3}\hbar^4$ has been subtracted. For ease of comparison, 2 $\hbar$ has been added to the data for ^{122,124}Ce and to the $\nu(d_{5/2})$ bands of ^{127,129}Ce.

VII. SUMMARY

In summary, excited states have been observed for the first time in the very neutron-deficient $Z = 58$ ^{123}Ce nucleus, using the ^{64}Zn(^{64}Zn,αn) reaction. The states have been assigned to ^{123}Ce by measuring properties of de-excitation γ rays in coincidence with evaporated neutrons, protons, and α particles. Three rotational bands have been observed, each consisting of at least eight $E2$ transitions. Two bands are possibly positive-parity signature partners based on the $\nu(g_{7/2})[413]5/2^+$ ($\alpha = \pm 1/2$) orbitals, and the third is tentatively proposed to have negative parity, based on the $\nu(h_{11/2})[532]5/2^-$ ($\alpha = -1/2$) orbital. A study of aligned angular momenta, in comparison to neighboring nuclei and to the results of cranked shell-model calculations, suggests that each of the bands exhibits the rotational alignment of a pair of $h_{11/2}$ protons at rotational frequency of 0.36 MeV/$\hbar$.

With the proposed tentative configurations and spin assignments, it appears that the bands in ^{123}Ce are more deformed than those in ^{125}Ce, in agreement with theoretical predictions. The assigned spins are consistent with the previously proposed ground-state spin of 5/2. Also, the observed rotational alignments of $h_{11/2}$ protons agree with cranked shell-model predictions. However, the nonobservation of $M1/E2$ transitions between bands assigned to be signature partners is difficult to explain, particularly if the band has the same configuration as the most intense positive-parity band in the neighboring isotope ^{125}Ce. A future study of the bands, at higher spins, will help clarify the configuration assignments. In particular, blocking of the lowest $h_{11/2}$ neutron alignment will be a useful test of the proposed configuration assignments. It would be very interesting to search for interband $M1/E2$ transitions between Bands 1 and 2, which would confirm their interpretation as signature partners.

ACKNOWLEDGMENTS

This work is supported in part by the NSF, the Engineering and Physical Sciences Research Council Science and Technology Facilities Council (UK), and by the Department of Energy, Office of Nuclear Physics, under Contract No. DE-AC02-06CH11357 (ANL) and Grant No. DE-FG02-88ER-40406 (Washington University). J. F. S. acknowledges support from the Scottish Universities Physics Alliance.

[1] P. J. Woods and C. N. Davids, Annu. Rev. Nucl. Part. Sci. **47**, 541 (1997).
[2] J. Dobaczewski, I. Hamamoto, W. Nazarewicz, and J. A. Sheikh, Phys. Rev. Lett. **72**, 981 (1994).
[3] C. J. Lister, B. J. Varley, R. Moscrop, W. Gelletly, P. J. Nolan, D. J. G. Love, P. J. Bishop, A. Kirwan, D. J. Thornley, L. Ying, R. Wadsworth, J. M. O'Donnell, H. G. Price, and A. H. Nelson, Phys. Rev. Lett. **55**, 810 (1985).
[4] J. F. Smith, V. Medina-Chico, C. J. Chiara, M. P. Carpenter, C. N. Davids, M. Devlin, J. L. Durell, D. B. Fossan, S. J. Freeman, R. V. F. Janssens, D. R. LaFosse, M. J. Leddy, P. Reiter, D. G. Sarantites, D. Seweryniak, K. Starosta, R. Wadsworth, A. N. Wilson, and J. N. Wilson, Phys. Rev. C **69**, 034339 (2004).
[5] A. N. Wilson, R. Wadsworth, J. F. Smith, S. J. Freeman, M. J. Leddy, C. J. Chiara, D. B. Fossan, D. R. LaFosse, K. Starosta, M. Devlin, D. G. Sarantites, J. N. Wilson, M. P. Carpenter, C. N. Davids, R. V. F. Janssens, D. Seweryniak, and R. Wyss, Phys. Rev. C **63**, 054307 (2001).
[6] P. Möller, J. R. Nix, W. D. Myers, and W. J. Swiatecki, At. Data Nucl. Data Tables **59**, 185 (1995).
[7] T. Duguet, P. Bonche, P.-H. Heenen, and J. Meyer, Phys. Rev. C **65**, 014310 (2001).
[8] P. J. Nolan, F. A. Beck, and D. B. Fossan, Annu. Rev. Nucl. Part. Sci. **44**, 561 (1994).
[9] D. G. Sarantites, P.-F. Hua, M. Devlin, L. G. Sobotka, J. Elson, J. T. Hood, D. R. LaFosse, J. E. Sarantites, and M. R. Maier, Nucl. Instrum. Methods Phys. Res. A **381**, 418 (1996).
[10] http://www.chemistry.wustl.edu/~dgs/mball/.
[11] D. G. Sarantites, W. Reviol, C. J. Chiara, R. J. Charity, L. G. Sobotka, M. Devlin, M. Furlotti, O. L. Pechenaya, J. Elson, P. Hausladen, S. Fischer, D. Balamuth, and R. M. Clark, Nucl. Instrum. Methods Phys. Res. A **530**, 473 (2004).
[12] http://www.chemistry.wustl.edu/~dgs/NeutronShell/.
[13] C. N. Davids, B. B. Back, K. Bindra, D. J. Henderson, W. Kutschera, T. Lauritsen, Y. Nagame, P. Sugathan, A. V. Ramayya, and W. B. Walters, Nucl. Instrum. Methods Phys. Res. B **70**, 358 (1992).
[14] J. F. Smith, C. J. Chiara, M. P. Carpenter, H. J. Chantler, P. T. W. Choy, C. N. Davids, M. Devlin, J. L. Durell, D. B. Fossan, S. J. Freeman, R. V. F. Janssens, N. S. Kelsall, T. Koike, D. R. LaFosse, E. S. Paul, P. Reiter, D. G. Sarantites, D. Seweryniak, K. Starosta, R. Wadsworth, A. N. Wilson, and P.-H. Heenen, Phys. Lett. B **625**, 203 (2005).
[15] E. S. Paul, A. J. Boston, A. Galindo-Uribarri, T. N. Ginter, C. J. Gross, A. N. James, P. J. Nolan, R. D. Page, S. D. Paul, A. Piechaczek, D. C. Radford, W. Reviol, L. L. Riedinger, H. C. Scraggs, W. Weintraub, and C.-H. Yu, Phys. Rev. C **58**, 801 (1998).
[16] C. M. Petrache, G. Lo Bianco, P. G. Bizzeti, A. M. Bizzeti-Sona, D. Bazzacco, S. Lunardi, M. Nespolo, G. de Angelis, P. Spolaore, N. Blasi, S. Brant, V. Krstic, and D. Vretenar, Eur. Phys. J. A **14**, 439 (2002).
[17] C. M. Petrache, G. Lo Bianco, P. G. Bizzeti, A. M. Bizzeti-Sona, D. Bazzacco, S. Lunardi, M. Nespolo, G. de Angelis, D. R. Napoli, N. Blasi, S. Brant, and D. Vretenar, Eur. Phys. J. A **16**, 337 (2003).
[18] B. M. Nyakó, J. Gizon, V. Barci, A. Gizon, S. Andre, D. Barnéoud, D. Curien, J. Genevey, and J. C. Merdinger, Z. Phys. A **334**, 513 (1989).
[19] E. S. Paul, J. P. Revill, M. Mustafa, S. V. Rigby, A. J. Boston, C. Foin, J. Genevey, A. Gizon, J. Gizon, I. M. Hibbert, D. T. Joss, P. J. Nolan, B. M. Nyakó, N. J. O'Brien, C. M. Parry, A. T. Semple, S. L. Shepherd, J. Timár, R. Wadsworth, and L. Zolnai, Phys. Rev. C **80**, 054312 (2009).

[20] E. S. Paul, P. Bednarczyk, A. J. Boston, C. J. Chiara, C. Foin, D. B. Fossan, J. Genevey, A. Gizon, J. Gizon, D. G. Jenkins, N. Kelsall, N. Kintz, T. Koike, D. R. LaFosse, P. J. Nolan, B. M. Nyakó, C. M. Parry, J. A. Sampson, A. T. Semple, K. Starosta, J. Timár, R. Wadsworth, A. N. Wilson, and L. Zolnai, Nucl. Phys. A **676**, 32 (2000).

[21] A. Galindo-Uribarri, S. M. Mullins, D. Ward, M. Cromaz, J. DeGraaf, T. E. Drake, S. Flibotte, V. P. Janzen, D. C. Radford, and I. Ragnarsson, Phys. Rev. C **54**, R454 (1996).

[22] D. M. Todd, R. Aryaeinejad, D. J. G. Love, A. H. Nelson, P. J. Nolan, P. J. Smith, and P. J. Twin, J. Phys. G (London) **10**, 1407 (1984).

[23] M. Palacz, Z. Sujkowski, J. Nyberg, J. Bacelar, J. Jongman, W. Urban, W. Hesselink, J. Nasser, A. Plompen, and R. Wyss, Z. Phys. A **338**, 467 (1991).

[24] E. S. Paul, A. J. Boston, D. T. Joss, P. J. Nolan, J. A. Sampson, A. T. Semple, F. Farget, A. Gizon, J. Gizon, D. Santos, B. M. Nyakó, N. J. O'Brien, C. M. Parry, and R. Wadsworth, Nucl. Phys. A **619**, 177 (1997).

[25] J. M. Nitschke, P. A. Wilmarth, P. K. Lemmertz, W.-D. Zeitz, and J. A. Honkanen, Z. Phys. A **316**, 249 (1984).

[26] A. M. Fletcher, Ph.D. thesis, University of Manchester, 2003.

[27] A. D. Gill, M. Sc. thesis, University of Manchester, 2005.

[28] H. J. Chantler, E. S. Paul, A. J. Boston, M. P. Carpenter, R. Charity, C. J. Chiara, P. T. W. Choy, C. N. Davids, M. Devlin, A. M. Fletcher, D. B. Fossan, D. G. Jenkins, N. S. Kelsall, T. Koike, D. R. LaFosse, P. J. Nolan, D. G. Sarantites, D. Seweryniak, J. F. Smith, K. Starosta, R. Wadsworth, and A. N. Wilson, Phys. Rev. C **66**, 014311 (2002).

[29] F. Plasil and M. Blann, Phys. Rev. C **11**, 508 (1975).

[30] J. F. Smith, C. J. Chiara, M. P. Carpenter, H. J. Chantler, P. T. W. Choy, C. N. Davids, M. Devlin, J. L. Durell, D. B. Fossan, S. J. Freeman, R. V. F. Janssens, N. S. Kelsall, T. Koike, D. R. LaFosse, E. S. Paul, D. G. Sarantites, D. Seweryniak, K. Starosta, R. Wadsworth, and A. N. Wilson (unpublished).

[31] D. C. Radford, Nucl. Instrum. Methods Phys. Res. A **361**, 297 (1995).

[32] D. C. Radford, Nucl. Instrum. Methods Phys. Res. A **361**, 306 (1995).

[33] A. G. Smith (private communication).

[34] J. F. Smith, C. J. Chiara, D. B. Fossan, G. J. Lane, J. M. Sears, I. Thorslund, H. Amro, C. N. Davids, R. V. F. Janssens, D. Seweryniak, I. M. Hibbert, R. Wadsworth, I. Y. Lee, A. O. Macchiavelli, A. V. Afanasjev, and I. Ragnarsson, Phys. Rev. C **61**, 044329 (2000).

[35] B. Cederwall, A. Johnson, B. Fant, S. Juutinen, P. Ahonen, S. Mitarai, J. Mukai, and J. Nyberg, Z. Phys. A **338**, 463 (1991).

[36] F. Lidén, L. Hildingsson, Th. Lindblad, J. Gizon, D. Barnéoud, and J. Gascon, Nucl. Phys. A **524**, 141 (1991).

[37] G. Garcia-Bermudez, M. A. Cardona, A. Filevich, R. V. Ribas, H. Somacal, and L. Szybisz, Phys. Rev. C **59**, 1999 (1999).

[38] R. Bengtsson and S. Frauendorf, Nucl. Phys. A **327**, 139 (1979).

[39] S. M. Harris, Phys. Rev. **138**, B509 (1965).

[40] R. Wyss, A. Granderath, R. Bengtsson, P. von Brentano, A. Dewald, A. Gelberg, A. Gizon, J. Gizon, S. Harissopulos, A. Johnson, W. Lieberz, W. Nazarewicz, J. Nyberg, and K. Schiffer, Nucl. Phys. A **505**, 337 (1989).

[41] A. Granderath, P. F. Mantica, R. Bengtsson, R. Wyss, P. von Brentano, A. Gelberg, and F. Seiffert, Nucl. Phys. A **597**, 427 (1996).

[42] R. Wyss, J. Nyberg, A. Johnson, R. Bengtsson, and W. Nazarewicz, Phys. Lett. B **215**, 211 (1988).

[43] W. Nazarewicz, R. Wyss, and A. Johnson, Nucl. Phys. A **503**, 285 (1989).

[44] W. Nazarewicz, J. Dudek, R. Bengtsson, and I. Ragnarsson, Nucl. Phys. A **435**, 397 (1985).

[45] S. Ćwiok, J. Dudek, W. Nazarewicz, W. Skalski, and T. Werner, Comput. Phys. Commun. **46**, 379 (1987).

[46] B. Sun, Yu. A. Litvinov, P. M. Walker, K. Beckert, P. Beller, F. Bosch, D. Boutin, C. Brandau, L. Chen, C. Dimopoulou, H. Geissel, R. Knöbel, C. Kozhuharov, J. Kurcewicz, S. A. Litvinov, A. Mazzocco, J. Meng, C. Nociforo, F. Nolden, W. R. Plass, C. Scheidenberger, M. Steck, H. Weick, and M. Winkler, Eur. Phys. J. A **31**, 393 (2007).

[47] B. Cederwall, A. Johnson, R. Wyss, C. G. Lindén, S. Mitari, J. Mukai, B. Fant, S. Juutinen, P. Ahonen, and J. Nyberg, Nucl. Phys. A **529**, 410 (1991).

[48] H. C. Scraggs, E. S. Paul, A. J. Boston, J. F. C. Cocks, D. M. Cullen, K. Helariutta, P. M. Jones, R. Julin, S. Juutinen, H. Kankaanpää, M. Muikku, P. J. Nolan, C. M. Parry, A. Savelius, R. Wadsworth, A. V. Afanasjev, and I. Ragnarsson, Nucl. Phys. A **640**, 337 (1998).